CHEMISTRY OF MATERIALS

Open Access

pubs.acs.org/cm

Article

Phase Diagram and Dielectric Response of Hybrid Lead Halide Hollow Perovskites: A Universal Behavior of Molecular Cation Mixing

Gabrielius Rimkus, Sergejus Balčiūnas, Maciej Ptak, Szymon Smółka, Vytautas Klimavičius, Daria Szewczyk, Adam Sieradzki, Vidmantas Kalendra, Jūras Banys, Mirosław Mączka, and Mantas Simėnas*

Cite This: *Chem. Mater.* 2024, 36, 7397−7405

Read Online

ACCESS | Metrics & More | Article Recommendations | Supporting Information

ABSTRACT: Mixing of molecular cations in hybrid lead halide perovskites is used to effectively tune the stability and performance of the photovoltaic devices based on these compounds. Upon introduction of bulky molecular cations such as ethylenediammonium (EN), the perovskite framework becomes locally broken resulting in so-called hollow perovskites. Here, we use a set of different experimental techniques to probe the structural phase transitions, molecular cation dynamics, and dielectric response in methylammonium-based $MA_{1-x}EN_xPb_{1-0.7x}I_{3-0.4x}$ hollow perovskites containing different amounts of EN molecular cations ($x \leq 0.26$). We determine the temperature−composition phase diagram of this system and show that the introduction of EN results in stabilization of the desirable high-symmetry cubic phase, as the structural phase transitions become partially suppressed. Broadband dielectric spectroscopy experiments are used to study the dynamics of molecular cations for different fractions of EN. For high levels of EN, we observe signatures of a dipolar glass phase formation. Our findings indicate a universal trend of the dielectric response upon molecular cation mixing independent of the size and charge of the incorporated guest cations in $MAPbI_3$.

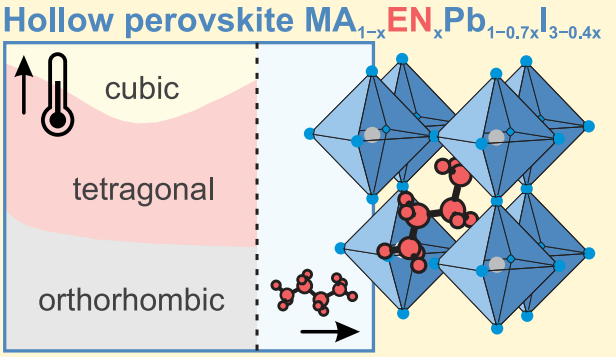

INTRODUCTION

Hybrid methylammonium (MA, $CH_3NH_3^+$) lead halide perovskites $MAPbX_3$ (X = I, Br, Cl) are extensively studied as efficient and solution-processable materials for photovoltaic applications.[1,2] In the recent decade, there has been an extraordinary advancement in the power conversion efficiency of solar cells relying on these compounds, with the current levels exceeding an impressive 25%.[3−8] The exceptional performance of these materials is related to key physical properties including a large absorption coefficient,[9] optimal band gap,[10] long carrier diffusion length,[11,12] low exciton binding energy,[13] and defect tolerance.[14] Some of these properties and consequently the device performance are significantly influenced by the dynamics of the molecular cations and structural phase transitions occurring in these compounds.[10,15−20]

The highest stability and performance of photovoltaic devices based on hybrid perovskites are achieved using compounds with mixed cations at the A-site.[21,22] Formamidinium (FA, $HC(NH_2)_2^+$)[7,8,23] and Cs^+[24] are the most popular alternatives to MA, although other cations such as dimethylammonium (DMA, $(CH_3)_2NH_2^+$),[25−27] ethylammoniumm (EA, $CH_3CH_2NH_3^+$),[28−34] methylhydrazinium (MHy, $CH_3NH_2NH_2^+$),[35−37] aziridinium (AZR, $CH_2CH_2NH_2^+$),[38,39] and Rb^+[40] are also gaining significant attention. Due to their effective radii being relatively similar to that of the MA,[41] it is generally feasible to accommodate a considerable fraction of these cations without significantly disrupting the 3D perovskite structure of $MAPbX_3$.[42]

Recently, several groups have demonstrated that much bigger molecular cations can be also incorporated, while preserving the overall 3D architecture.[43−51] In this context, two new families of compounds have emerged: so-called lead- and iodide-deficient perovskites accommodating a substantial amount of bulky molecular cations such as hydroxyethylammonium and thioethylammonium,[49−52] and hollow perovskites with general formula $A_{1-x}B_xM_{1-0.7x}X_{3-0.4x}$ (A =

Received: May 9, 2024
Revised: June 18, 2024
Accepted: July 9, 2024
Published: July 23, 2024

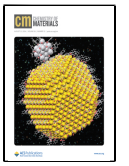

MA, FA; B = ethylenediammonium (EN, $NH_3CH_2CH_2NH_3^{2+}$), propylenediammonium, trimethylenediammonium; M = Pb, Sn; X = I, Br).[43−47,53] It was found that the hosting of such cations results in the removal of neighboring metal halide moieties from the crystal lattice, generating vacancy defects in the 3D perovskite network. The deficient perovskites such as d-$MAPbI_3$ were found to form lead- and iodide-deficient frameworks with periodic distribution of defects,[49−51] while, on the other hand, the defect distribution in hollow perovskites was determined to be irregular.[47,53]

The formation of such highly defective hybrid perovskites proved to be a successful strategy to enhance the photovoltaic properties,[43,44,46,48,53,54] significantly increase stability,[43−46,48,50,51,55] and suppress ion migration[56,57] in these compounds. However, the impact of large cation incorporation and corresponding disruption of the lattice on the structural phase transitions and overall dynamics in the system remains unexplored despite a tight connection of these phenomena with the photovoltaic properties and stability of hybrid perovskites.

In this work, we use a suite of experimental techniques to study how introduction of EN cations affects the structural phase transitions, broadband dielectric response and molecular cation dynamics in $MA_{1-x}EN_xPb_{1-0.7x}I_{3-0.4x}$ hollow hybrid perovskite family. We determine the temperature−concentration phase diagram of these compounds, which reveals that the structural phase transitions are partially suppressed for higher levels of EN resulting in stabilization of the cubic phase. We also observe signatures of the dipolar glass phase indicating a significant change in the molecular cation dynamics and long-range order upon mixing. Our findings also indicate that the dielectric response of hollow perovskites are very similar to other mixed perovskite systems that contain smaller monovalent guest cations pointing to a universal mixing behavior.

EXPERIMENTAL DETAILS

Sample Synthesis. Single crystals of $MAPbI_3$ doped with EN cations were grown by dissolving 4 mmol of PbI_2, and stoichiometric amounts of methylamine (2 M solution in methanol, Sigma-Aldrich) and ethylenediamine (99.5%, Sigma-Aldrich) in a mixture of propylene carbonate (PC, 99.7%, Sigma-Aldrich) and HI (57 wt % in H_2O, stabilized with H_3PO_2, Sigma-Aldrich) under stirring on a hot plate (50°C). The PC:HI volume ratio was 2.6:1, and the total amount of methylamine and ethylenediamine was 4 mmol. The clear solution was transferred into a glass vial, which was kept at 75°C. The black crystals were separated from the liquid after a few days and dried at room temperature. Based on the previous report,[47] we assign the chemical formula of the mixed compounds to $MA_{1-x}EN_xPb_{1-0.7x}I_{3-0.4x}$. The following EN cation fractions were obtained in the synthesized solid-solutions using ^{1}H NMR spectroscopy: x = 0.02, 0.04, 0.12, 0.15, and 0.26.

We have also tried to obtain the samples using a similar procedure as reported in ref 47 with the difference that we used PbI_2 instead of lead acetate as a source of lead. In this method, 3 mmol of PbI_2 was dissolved in 5 mL of HI under magnetic stirring at about 100 °C. Then appropriate amount of ethylenediamine was dissolved at room temperature in 1.2 mL of H_3PO_2, and this solution was added to the hot solution of PbI_2 in HI. In the next step, 3 mmol of methylamine hydrochloride was added to the reaction mixture. The small crystals formed in the solution were collected by filtration and dried at room temperature. The amount of methylamine hydrochloride was constant (3 mmol) for all samples, but various amounts of ethylenediamine were used, i.e., 0.6, 0.9, 1.2, 1.5, 1.8, 2.1, and 3 mmol. The highest amount of ethylenediamine used in our synthesis was the same as in literature, but the PXRD patterns showed that for the higher ethylenediamine content in the reaction mixture, the samples contain a significant amount of the impurity phase. Therefore, in our studies we used only the samples prepared using the first method.

NMR. ^{1}H NMR experiments were carried out at 14.1 T on a Bruker Avance Neo NMR spectrometer operating at 600.3 MHz using a 5 mm Bruker ^{1}H−^{13}C−BB TBI probe. Temperature was stabilized at 298 K. A pulse sequence employing 10 μs $\pi/6$ excitation pulse followed by a 5 s repetition delay was employed, and 64 scans were accumulated. Samples were dissolved in DMSO-d_6 (99.96% D atom, Sigma-Aldrich), which was used for a lock. The amount x of EN cations in $MA_{1-x}EN_xPb_{1-0.7x}I_{3-0.4x}$ was determined by comparing the intensities of a methyl group signal of MA (δ = 2.37 ppm) and a methylene signal of EN (δ = 3.01 ppm).

PXRD. Powder X-ray diffraction (PXRD) patterns of the ground crystals were measured in the reflection mode using an X'Pert PRO X-ray diffraction system equipped with a PIXcel ultrafast line detector and Soller slits for Cu Kα_1 radiation (λ = 1.54056 Å).

DSC. The differential scanning calorimetry (DSC) experiments of powder samples were performed using a Mettler Toledo DSC-3 calorimeter with a resolution of 0.4 μW. Nitrogen was used as a purging gas, and the heating/cooling rate was 5 K/min.

C_p Measurements. The heat capacity C_p was measured using a Physical Property Measurement System (PPMS) from Quantum Design implementing the thermal relaxation method.[58] The experiment was performed on single crystalline samples with mass ranging from 2.8 to 4.2 mg. In the case of very small crystals, 3−5 crystals were used in order to increase the signal response during the experiment. In the vicinity of the structural phase transitions, a fine temperature step was used.

Raman Spectroscopy. Room-temperature Raman spectra were measured for powdered crystals using a Bruker FT 100/S spectrometer with YAG:Nd laser excitation (λ = 1064 nm) and 2 cm^{-1} spectral resolution.

Infrared Spectroscopy. IR spectra were measured in the 7−330 K temperature range using a Nicolet iS50 FT-IR spectrometer and a closed cycle CS202AE-DMX-1AL cryostat (Advanced Research Systems) equipped with thallium bromoiodide (KRS-5) windows. The samples were prepared using a standard KBr pellet method, and the spectral resolution was 2 cm^{-1}.

Dielectric Spectroscopy. Broadband dielectric spectroscopy experiments were performed in the 100 Hz−1 MHz frequency range using an HP4284A LCR meter. A flat capacitor model was used to calculate the complex dielectric permittivity from the measured capacitance and loss tangent of pressed pellet samples. Temperature-dependent dielectric spectra were measured on cooling at a rate less than 1 K/min. Silver paste was used for sample electrodes.

RESULTS AND DISCUSSION

We studied $MA_{1-x}EN_xPb_{1-0.7x}I_{3-0.4x}$ hollow perovskites with the EN fractions of x = 0, 0.02, 0.04, 0.12, 0.15, and 0.26, as determined by the ^{1}H NMR spectroscopy (see Figure S1, Supporting Information). We were not able to obtain higher incorporation indicating that the EN solubility limit in $MAPbI_3$ is about 26% using this synthesis method. We also performed initial sample characterization using room-temperature Raman spectroscopy, which revealed a monotonous increase of the EN band intensity with increasing x (Figure S2). The PXRD patterns of the obtained samples are summarized in Figure S3 showing that for higher mixing levels (x > 0.12) the room-temperature crystal symmetry changes from tetragonal to cubic (see the Supporting Information for more details) in a good agreement with the previous study.[47] In addition, the unit cell volume of the studied compounds experiences a very similar linear increase with the EN content (Figure S4) as was observed in the previous work[47] confirming that our studied compositions can be described by $MA_{1-x}EN_xPb_{1-0.7x}I_{3-0.4x}$ formula. The initial characterization of the samples shows

https://doi.org/10.1021/acs.chemmater.4c01346
Chem. Mater. 2024, 36, 7397−7405

that the EN cations were successfully incorporated in the crystal structure of $MAPbI_3$, while maintaining the overall 3D perovskite architecture.

We further investigated the behavior of the structural phase transitions and dynamics in $MA_{1-x}EN_xPb_{1-0.7x}I_{3-0.4x}$ using different experimental techniques including DSC, heat capacity measurements, IR as well as dielectric spectroscopies. Our previous studies proved that such a broad variety of complementary experimental tools is necessary to map the intricate phase diagrams and dynamics of mixed lead halide perovskites.[23,27,34,37,39,42]

The measured heat capacity C_p and DSC data are presented in Figure 1a,b. For the nonmixed $MAPbI_3$ compound, two phase transitions can be observed at 329 and 157 K corresponding to the cubic-tetragonal and tetragonal-orthorhombic symmetry lowering, respectively.[42] For low mixing levels (x = 0.02 and 0.04), a clear decrease in the temperatures of both phase transitions can be observed indicating that the presence of EN cations impedes the ordering of the system. Note that here we assume the same sequence of the symmetry lowering in the mixed compositions as in $MAPbI_3$. For the intermediate fractions of EN (x = 0.12 and 0.15), the temperature of the cubic−tetragonal phase transitions exhibits further lowering (Figure 1b), while the tetragonal−orthorhombic phase transition is no longer resolved (Figure 1a). Interestingly, for the highest mixing level (x = 0.26), the anomaly of the low-temperature phase transition reappears at 118 K (Figure 1a). In addition, for this compound, the temperature of the cubic-tetragonal transition recovers and reaches a value of about 300 K (see Figures 1b and S5).

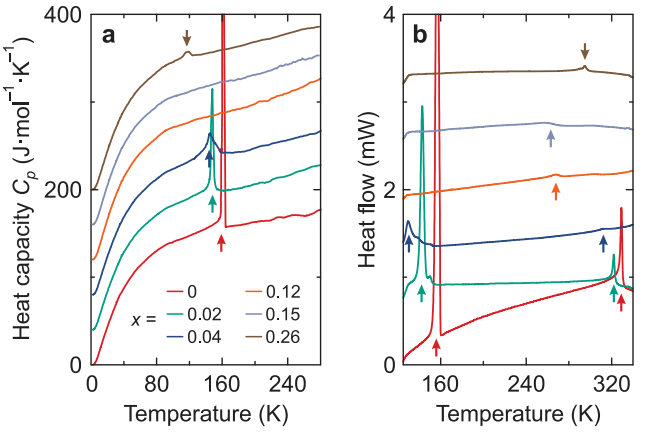

Figure 1. Temperature dependence of the (a) heat capacity and (b) DSC traces of $MA_{1-x}EN_xPb_{1-0.7x}I_{3-0.4x}$ perovskites. Curves are offset by an arbitrary shift for clarity. Clearly resolved anomalies of the phase transitions are indicated by the arrows.

The absence of clear low-temperature anomalies in the C_p data of the x = 0.12 and 0.15 samples may indicate that the tetragonal−orthorhombic phase transition becomes fully suppressed upon mixing, as was also observed in other similar highly mixed systems such as MA/$DMAPbBr_3$[27] and MA/$EAPbI_3$.[34] However, the observation of the low-temperature phase transition in the x = 0.26 compound implies that the phase transition may not be fully suppressed. Thus, to clarify this region of the phase diagram and gain insight about the lattice as well as molecular cation ordering, we also performed temperature-dependent IR spectroscopy experiments of the x = 0.02, 0.12, 0.15, and 0.26 samples. The IR spectra in the 3300−800 cm^{-1} range measured at different temperatures are presented in Figure 2. The most intense bands correspond to vibrations of MA cations, and their assignment (Figure 2a) is based on previous room-temperature IR study of $MAPbI_3$.[59] The spectra also show several weak bands at 1329, 1312, 1025,

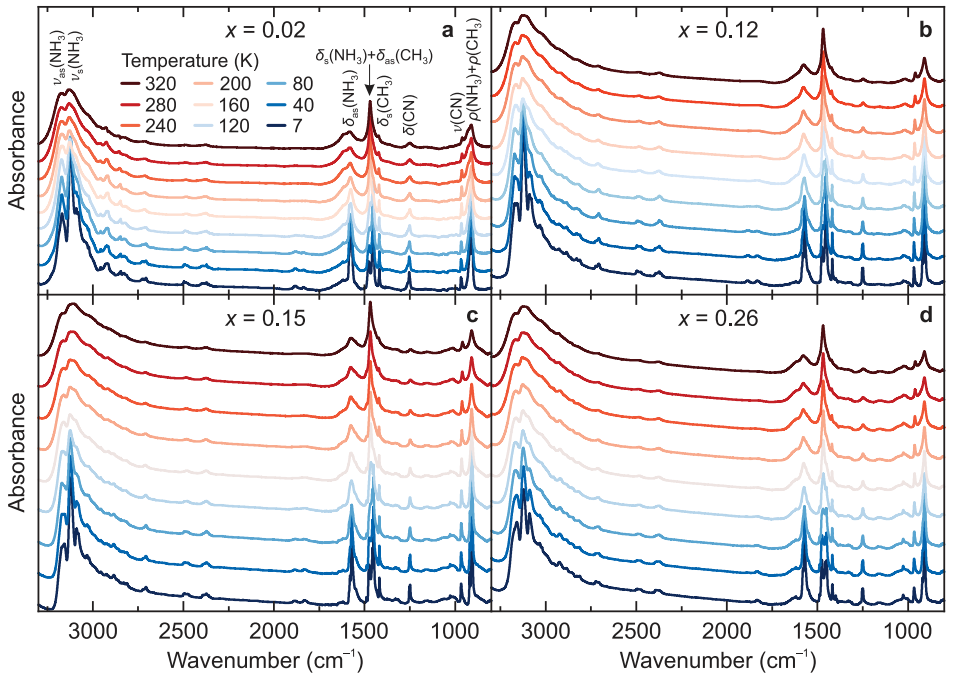

Figure 2. Temperature-dependent IR spectra of the (a) x = 0.02, (b) 0.12, (c) 0.15 and (d) 0.26 samples in the 3300−800 cm^{-1} range. The most intense vibrations of MA cations and their assignments are presented in (a).

https://doi.org/10.1021/acs.chemmater.4c01346
Chem. Mater. 2024, 36, 7397−7405

and 1011 cm^{-1}, which we assign to a small fraction of the $ENPbI_4$ impurity phase.

The temperature dependences of the IR band wavenumbers are presented in Figures S7 and S8, while Figure 3 shows a detailed temperature evolution of the IR absorbance in the 1490−1410 cm^{-1} range. For the weakly mixed compound (x = 0.02), a weak shift and a gradual narrowing of the IR bands on cooling down to 140 K can be observed. Below this temperature, the IR spectrum exhibits abrupt changes (see Figures 3, S7a, and S8a). First, the IR bands exhibit pronounced narrowing and change of relative intensity. This behavior is especially pronounced for the NH_3 stretching ($\nu_{as}(NH_3)$ and $\nu_s(NH_3)$), NH_3 bending ($\delta_{as}(NH_3)$ and $\delta_s(NH_3)$), and coupled NH_3+CH_3 rocking ($\rho_{as}(NH_3)$ + $\rho_{as}(CH_3)$) modes. For instance, the intensity of the ∼1450 cm^{-1} band strongly increases, and this band narrows (Figure 3). Second, many bands split, and new bands appear below 140 K. For example, one clear band at 1450.3 cm^{-1} and one very weak band at 1455.7 cm^{-1} are split into four bands at 1450.3, 1453.9, 1456.6, and 1462.1 cm^{-1} (Figures 3 and S7a), and the ν(CN) singlet splits into a doublet (964.5 + 968.2 cm^{-1}, Figure S8a). Furthermore, a new band appears at 916.9 cm^{-1} (Figure S8a). Third, many IR modes exhibit highly pronounced shifts of their wavenumbers below 140 K (Figures 3, S7a, and S8a). For instance, the ∼1469 cm^{-1} band exhibits slight softening by 0.7 cm^{-1} on cooling from 320 to 140 K, followed by hardening by 6.4 cm^{-1} on further cooling below 140 K. The observed changes indicate that the weakly mixed x = 0.02 compound exhibits structural phase transition at about 140 K in a good agreement with the DSC and C_p data. The narrowing of the IR bands indicates that the phase transition involves freezing of the MA cation motion, while band splitting shows symmetry lowering.[42,60]

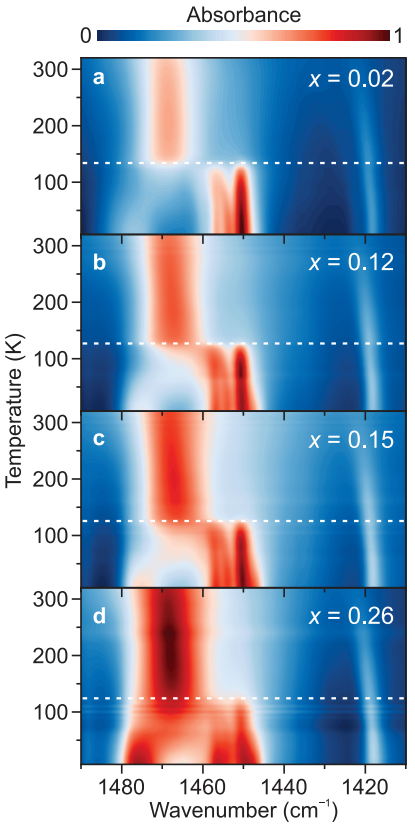

Figure 3. Absolute IR intensity in the 1490−1410 cm^{-1} range as a function of temperature for the x = 0.02, 0.12, 0.15, and 0.26 samples. Horizontal dashed lines denote the temperatures of the structural phase transitions.

Incorporation of a higher amount of EN into the structure of $MAPbI_3$ has significant effect on the IR spectra (Figures 2, 3, S7, and S8). First of all, higher mixing leads to broadening of the IR bands. This behavior is especially pronounced at higher temperatures for the band near 1470 cm^{-1} (see Figure 3). Note that at moderate mixing (x = 0.12 and 0.15), the IR spectra still show abrupt changes due to the tetragonal-orthorhombic phase transition, which was not resolved in the C_p data. The changes of the IR spectra are very similar to those observed for the sample with 2% of EN. The anomalies are observed at lower temperatures indicating partial suppression of the phase transitions. Moreover, the overall increase of intensity of the 1450 cm^{-1} mode at the phase transition point is less pronounced for moderately mixed compositions compared to the x = 0.02 sample (see Figure S7). For the highest EN fraction (x = 0.26), the changes of the IR spectra are less abrupt. For example, the intensity of the 1450 cm^{-1} mode exhibits only a weak change (Figure S7), although the heatmap presented in Figure 3d shows a clear phase transition indicating that the heavily mixed composition also experiences a distortion of the inorganic substructure and at least partial ordering of MA cations.

Our DSC, C_p and IR spectroscopy results allow us to fully map the temperature−concentration phase diagram of the $MA_{1-x}EN_xPb_{1-0.7x}I_{3-0.4x}$ system (see Figure 4a). The phase diagram clearly shows a partial stabilization of the cubic phase for the intermediate fractions of EN, where the cubic−tetragonal phase transition temperature decreases well below room temperature to about 260 K for x = 0.15. Such a lattice symmetrization[30,61] is important for applications of hollow perovskites in photovoltaic devices operating close to room

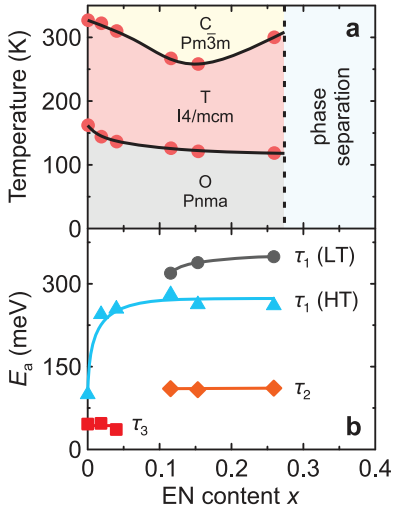

Figure 4. (a) Temperature−composition phase diagram of mixed $MA_{1-x}EN_xPb_{1-0.7x}I_{3-0.4x}$ perovskites. Dots indicate structural phase transition points as determined using different experimental techniques, while curves indicate tentative phase boundaries. Abbreviations: C, cubic; T, tetragonal; and O, orthorhombic. (b) EN concentration dependence of the activation energy E_a of different dipolar relaxation processes. Curves in (b) are guide for the eye. Error bars are smaller than data points.

https://doi.org/10.1021/acs.chemmater.4c01346
Chem. Mater. 2024, 36, 7397−7405

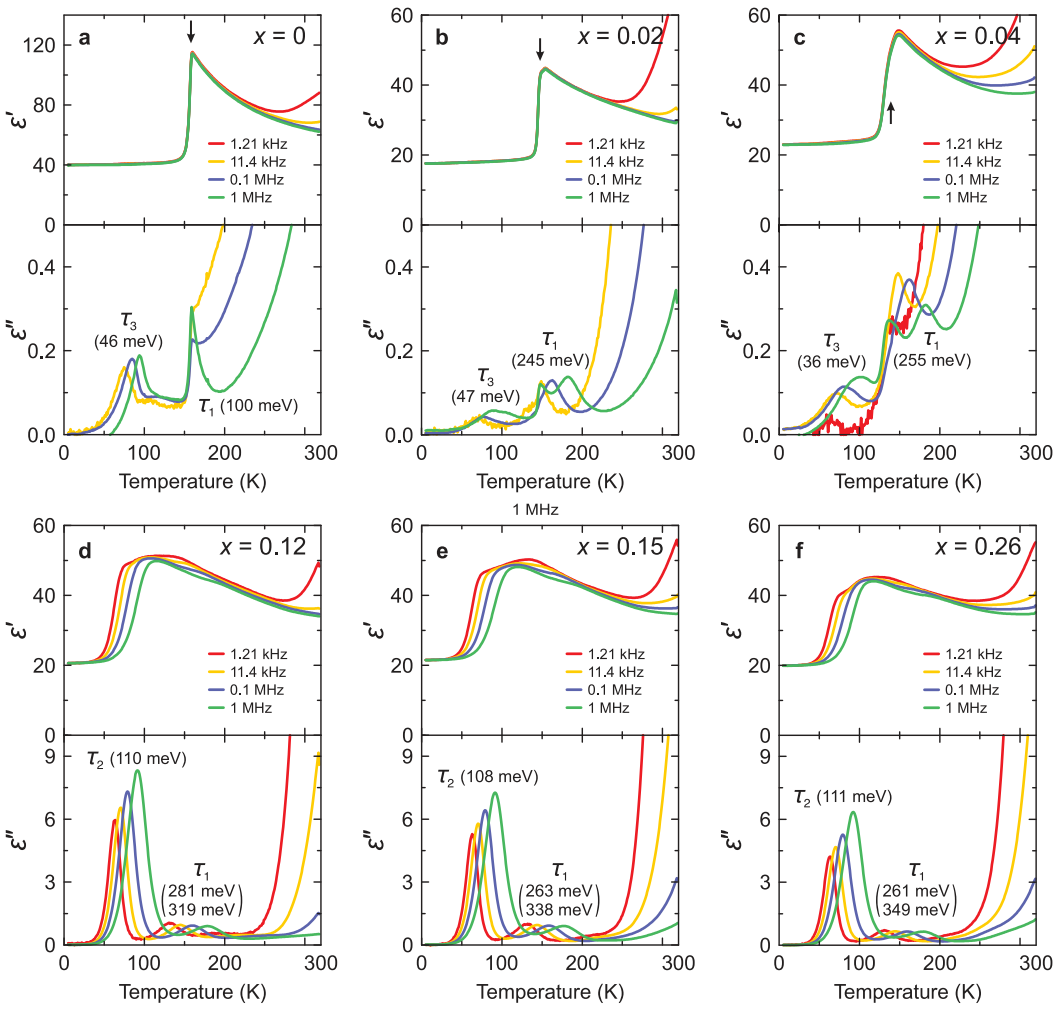

Figure 5. (a–f) Temperature dependence of the complex dielectric permittivity of $MA_{1-x}EN_xPb_{1-0.7x}I_{3-0.4x}$ pellet samples presented at selected frequencies. Arrows indicate resolved phase-transition anomalies. Different relaxation processes are indicated together with the determined activation energies. The value of activation energy for the τ_1 relaxation process in the $x = 0$ sample is taken from ref 17.

temperature, as, otherwise, a repetitive occurrence of the structural phase transition could accumulate fatigue and strain of the crystal lattice, which is harmful for device operation.[62]

The origin of the observed unusual recovery of the transition temperature of the cubic-tetragonal phase transition for the highest mixing level ($x = 0.26$) (Figure 4a) is unclear. We can discard the phase separation and EN cation clustering issue, as the temperature of the tetragonal-orthorhombic phase transition does not increase (Figure 4a), and the nonmixed $ENPbI_4$ compound does not exhibit any phase transitions in this temperature region (Figure S6). Thus, this points to a more complex phase transition mechanism presumably involving some cooperative ordering of the MA and EN cations for the highest mixing levels. We note that such a recovery of the phase transition temperature was also recently observed for the related MA/MHyPbI$_3$ system.[37]

We also note that our results show that the phase transitions are still present even for the highest level of EN cations. This is in contrast to the related mixed MA/EAPbI$_3$ system, where a complete suppression of the low-temperature phase transition was observed for the heavily mixed compositions with the EA fraction of 31% and 38%.[34] However, for the EA cation concentration of 21% (comparable to the highest level of EN studied in this work), the phase transition was still not completely suppressed. This suggests that the phase transition suppression in $MAPbI_3$ is mainly determined by the disruption of the MA cation ordering and not the inorganic framework disruption, which is expected to be much more pronounced in hollow perovskites for the same guest cation concentration.

We also performed broadband dielectric spectroscopy experiments on the pellet samples to study the molecular cation dynamics in the different regions of the phase diagram of $MA_{1-x}EN_xPb_{1-0.7x}I_{3-0.4x}$. The temperature dependence of the real ε' and imaginary ε'' (dielectric loss) parts of complex dielectric permittivity $\varepsilon^* = \varepsilon' - i\varepsilon''$ for all studied compositions is presented in Figure 5. For the nonmixed $MAPbI_3$ compound, the dielectric permittivity exhibits a sudden decrease at the tetragonal-orthorhombic phase transition point (Figure 5a), which is caused by the long-range cooperative ordering of the MA electric dipoles.[17,42,63−66] Upon introduction of a small amount of EN ($x = 0.02$ and 0.04), the temperature of the phase transition decreases, and the anomaly becomes broader (Figure 5b,c), in a good agreement with other experiments. For the higher EN incorporation ($x \geq 0.12$), the phase transition is no longer resolved in the dielectric data, as it is replaced by a broad dipolar relaxation (Figure 5d–f).

https://doi.org/10.1021/acs.chemmater.4c01346
Chem. Mater. 2024, 36, 7397−7405

The dielectric spectroscopy experiments also allowed us to observe and characterize different dipolar relaxation processes in the studied materials. Earlier studies indicated that the rotational motion of MA cations within the tetragonal phase of $MAPbI_3$ has an activation energy (rotation barrier) E_a of 100 meV[17] and occurs in the GHz frequency range.[67] In line with our previous work on the mixed MA/EAPbI$_3$ system,[34] we denote this process as τ_1 (Figure 5). With increasing x, this relaxation moves into the studied frequency window allowing us to probe this process in $MA_{1-x}EN_xPb_{1-0.7x}I_{3-0.4x}$ (Figure 5b−f; see the Supporting Information for the analysis of the frequency-domain data, Figures S9 and S10). The determined activation energies for all studied compositions are summarized in Figure 4b revealing a sudden and substantial increase of E_a to about ∼260 meV with increasing x. This indicates that introduction of EN significantly hinders the MA cation reorientation likely mediated via a severe disruption of the inorganic framework caused by much bigger EN cations. Note that a substantial increase of activation energies was also observed for other mixed perovskite systems[23,27,34,42] showing that this is a universal mixing effect.

A deeper analysis of the relaxation data (Figure S11) also revealed that the activation energy of the τ_1 process increases significantly as the system crosses the tetragonal-orthorhombic phase transition point (see Figure 4b). For instance, for the x = 0.26 compound, the difference is almost 100 meV (260 vs 349 meV) indicating that the phase transition further increases the barrier of MA reorientation in addition to the effect from the EN cations.

For low mixing levels ($x \leq 0.04$), we also observed an additional rather weak dipolar relaxation below 125 K, which we denote as τ_3. The activation energy of this process is close to 40 meV and seems to be independent of the EN fraction (Figure 4b). Such a weak relaxation is rather common in hybrid perovskites, as, in addition to $MAPbI_3$, it was also observed for the related nonmixed $FAPbI_3$[63] and recently reported $AZRPbX_3$ (X = Cl, Br, I)[39] compounds. The origin of this process is not fully understood, but it may be related to the twisting motion of MA cations, since this process has a similar E_a value of 60 meV, as reported by Xu et al. using magnetic resonance techniques.[68]

For a higher level of mixing ($x \geq 0.12$), the low-temperature process τ_3 is masked by a significantly stronger another dipolar relaxation (Figure 5d−f), which is denoted by τ_2. Compared to the τ_3 process, the τ_2 relaxation also has a much higher activation energy of about 110 meV, which is independent of the EN level (see Figure 4b). The appearance of this relaxation indicates a qualitatively different behavior of MA molecular cations in this region of the phase diagram. We note that this relaxation was previously observed in other highly mixed hybrid perovskite systems such as MA/DMAPbBr$_3$,[27] MA/FAPbBr$_3$,[23] MA/FAPbI$_3$,[66] and MA/EAPbI$_3$[34] demonstrating that this is a universal behavior independent of the introduced guest cations.

Such a broad dipolar relaxation is a signature of a dipolar glass phase formation due to the frustration of MA electric dipoles caused by the disrupted inorganic framework, which is frequently observed in mixed inorganic perovskite and related compounds.[69−71] A dipolar glass phase should exhibit freezing (divergence of the relaxation time) at some nonzero temperature described by a Vogel−Fulcher law.[70] However, we did not observe such a behavior as the simple Arrhenius law was sufficient to describe the temperature dependence of the τ_2 relaxation time (Figure S11). The absence of the deviation from the Arrhenius law suggests that the freezing of dipolar glass might occur at very low temperatures. We note that similar signatures of the glassy phase were also observed in other related highly mixed hybrid perovskite systems[23,27,34,42,66,72,73] indicating a universal behavior.

SUMMARY AND CONCLUSIONS

We used a suite of different experimental techniques to map the phase diagram and probe the molecular cation dynamics and dielectric response in $MA_{1-x}EN_xPb_{1-0.7x}I_{3-0.4x}$ hollow perovskites. The initial sample characterization revealed a successful incorporation of EN cations up to x = 0.26 concentration, beyond which we observed a phase separation.

The DSC and heat capacity experiments revealed a partial suppression of the structural phase transitions and thus increased stability of the cubic phase (lattice symmetrization). The maximum decrease of the cubic−tetragonal phase transition was obtained for the x = 0.15 EN concentration to a value of 260 K, which is below a typical operation temperature of photovoltaic devices. Interestingly, upon increase of the EN content to the maximum value of x = 0.26, the cubic−tetragonal phase transition recovered indicating a complex interplay between the MA and EN molecular cations. The temperature-dependent IR absorption measurements showed clear changes of the MA cation dynamics at the tetragonal-orthorhombic phase transition point allowing us to completely map the rest of the phase diagram.

The dielectric spectroscopy experiments revealed information on the evolution of the electric dipole dynamics upon introduction of EN in $MAPbI_3$. Depending on the EN fraction, we observed three distinct dielectric relaxation processes. For all mixing levels, we observed a reorientation of MA cations with the activation energy exhibiting a substantial increase with increase of EN. In addition, for low fractions of EN, a low-intensity process was observed in the low-temperature region, which may originate from a twisting motion of MA cations. The third process emerges and becomes dominant for high levels of EN. The temperature evolution of this relaxation suggests a formation of a dipolar glass phase with a very low freezing temperature.

Our results show that the overall evolution of the dielectric response of hybrid perovskites upon mixing is practically independent of the size and charge of a guest molecular cation. This points to a universal behavior of electric dipole frustration mediated by a substantial lattice strain created by mixing. We anticipate that such a universal behavior could also persist in hybrid perovskites mixed at the B-site.

Overall, our study provides insights into the structural phase transitions and dynamics of mixed lead halide perovskites, important for understanding their behavior in photovoltaic applications.

ASSOCIATED CONTENT

Supporting Information

The Supporting Information is available free of charge at https://pubs.acs.org/doi/10.1021/acs.chemmater.4c01346.

Additional NMR, Raman, PXRD, DSC, heat capacity, IR, and dielectric spectroscopy data (PDF)

https://doi.org/10.1021/acs.chemmater.4c01346
Chem. Mater. 2024, 36, 7397−7405

AUTHOR INFORMATION

Corresponding Author

Mantas Šimėnas − *Faculty of Physics, Vilnius University, LT-10257 Vilnius, Lithuania;* orcid.org/0000-0002-2733-2270; Email: mantas.simenas@ff.vu.lt

Authors

Gabrielius Rimkus − *Faculty of Physics, Vilnius University, LT-10257 Vilnius, Lithuania*

Sergejus Balčiūnas − *Faculty of Physics, Vilnius University, LT-10257 Vilnius, Lithuania*

Maciej Ptak − *Institute of Low Temperature and Structure Research, Polish Academy of Sciences, PL-50-422 Wroclaw, Poland;* orcid.org/0000-0002-4639-2367

Szymon Smółka − *Institute of Low Temperature and Structure Research, Polish Academy of Sciences, PL-50-422 Wroclaw, Poland*

Vytautas Klimavičius − *Institute of Chemical Physics, Vilnius University, LT-10257 Vilnius, Lithuania*

Daria Szewczyk − *Institute of Low Temperature and Structure Research, Polish Academy of Sciences, PL-50-422 Wroclaw, Poland;* orcid.org/0000-0001-7923-1239

Adam Sieradzki − *Department of Experimental Physics, Wroclaw University of Science and Technology, PL-50-370 Wroclaw, Poland;* orcid.org/0000-0003-4136-5754

Vidmantas Kalendra − *Faculty of Physics, Vilnius University, LT-10257 Vilnius, Lithuania*

Jūras Banys − *Faculty of Physics, Vilnius University, LT-10257 Vilnius, Lithuania*

Mirosław Mączka − *Institute of Low Temperature and Structure Research, Polish Academy of Sciences, PL-50-422 Wroclaw, Poland;* orcid.org/0000-0003-2978-1093

Complete contact information is available at: https://pubs.acs.org/10.1021/acs.chemmater.4c01346

Notes

The authors declare no competing financial interest.

ACKNOWLEDGMENTS

This project has been funded by the Lithuanian Academy of Sciences (Young Researcher Grant).

REFERENCES

(1) Snaith, H. J. Perovskites: The Emergence of a New Era for Low-Cost, High-Efficiency Solar Cells. *J. Phys. Chem. Lett.* **2013**, *4*, 3623−3630.

(2) Grätzel, M. The Light and Shade of Perovskite Solar Cells. *Nat. Mater.* **2014**, *13*, 838−842.

(3) Kojima, A.; Teshima, K.; Shirai, Y.; Miyasaka, T. Organometal Halide Perovskites as Visible-Light Sensitizers for Photovoltaic Cells. *J. Am. Chem. Soc.* **2009**, *131*, 6050−6051.

(4) Liu, M.; Johnston, M. B.; Snaith, H. J. Efficient Planar Heterojunction Perovskite Solar Cells by Vapour Deposition. *Nature* **2013**, *501*, 395−398.

(5) Park, N.-G. Organometal Perovskite Light Absorbers Toward a 20% Efficiency Low-Cost Solid-State Mesoscopic Solar Cell. *J. Phys. Chem. Lett.* **2013**, *4*, 2423−2429.

(6) Li, Z.; Klein, T. R.; Kim, D. H.; Yang, M.; Berry, J. J.; van Hest, M. F. A. M.; Zhu, K. Scalable Fabrication of Perovskite Solar Cells. *Nat. Rev. Mater.* **2018**, *3*, 18017.

(7) Jeong, J.; Kim, M.; Seo, J.; Lu, H.; Ahlawat, P.; Mishra, A.; Yang, Y.; Hope, M. A.; Eickemeyer, F. T.; Kim, M.; et al. Pseudo-Halide Anion Engineering for α-$FAPbI_3$ Perovskite Solar Cells. *Nature* **2021**, *592*, 381−385.

(8) Yoo, J. J.; Seo, G.; Chua, M. R.; Park, T. G.; Lu, Y.; Rotermund, F.; Kim, Y.-K.; Moon, C. S.; Jeon, N. J.; Correa-Baena, J.-P.; et al. Efficient Perovskite Solar Cells via Improved Carrier Management. *Nature* **2021**, *590*, 587−593.

(9) Manser, J. S.; Christians, J. A.; Kamat, P. V. Intriguing Optoelectronic Properties of Metal Halide Perovskites. *Chem. Rev.* **2016**, *116*, 12956−13008.

(10) Frost, J. M.; Butler, K. T.; Brivio, F.; Hendon, C. H.; van Schilfgaarde, M.; Walsh, A. Atomistic Origins of High-Performance in Hybrid Halide Perovskite Solar Cells. *Nano Lett.* **2014**, *14*, 2584−2590.

(11) Stranks, S. D.; Eperon, G. E.; Grancini, G.; Menelaou, C.; Alcocer, M. J. P.; Leijtens, T.; Herz, L. M.; Petrozza, A.; Snaith, H. J. Electron-Hole Diffusion Lengths Exceeding 1 Micrometer in an Organometal Trihalide Perovskite Absorber. *Science* **2013**, *342*, 341−344.

(12) Chen, T.; Chen, W.-L.; Foley, B. J.; Lee, J.; Ruff, J. P. C.; Ko, J. Y. P.; Brown, C. M.; Harriger, L. W.; Zhang, D.; Park, C. Origin of Long Lifetime of Band-Edge Charge Carriers in Organic-Inorganic Lead Iodide Perovskites. *Proc. Natl. Acad. Sci. U.S.A.* **2017**, *114*, 7519−7524.

(13) Miyata, A.; Mitioglu, A.; Plochocka, P.; Portugall, O.; Wang, J. T.-W.; Stranks, S. D.; Snaith, H. J.; Nicholas, R. J. Direct Measurement of the Exciton Binding Energy and Effective Masses for Charge Carriers in Organic-Inorganic Tri-Halide perovskites. *Nat. Phys.* **2015**, *11*, 582.

(14) Ball, J. M.; Petrozza, A. Defects in Perovskite-Halides and their Effects in Solar Cells. *Nat. Energy* **2016**, *1*, 16149.

(15) Frost, J. M.; Walsh, A. What Is Moving in Hybrid Halide Perovskite Solar Cells? *Acc. Chem. Res.* **2016**, *49*, 528−535.

(16) Egger, D. A.; Rappe, A. M.; Kronik, L. Hybrid Organic-Inorganic Perovskites on the Move. *Acc. Chem. Res.* **2016**, *49*, 573−581.

(17) Anusca, I.; Balčiūnas, S.; Gemeiner, P.; Svirskas, S.; Sanlialp, M.; Lackner, G.; Fettkenhauer, C.; Belovickis, J.; Samulionis, V.; Ivanov, M.; et al. Dielectric Response: Answer to Many Questions in the Methylammonium Lead Halide Solar Cell Absorbers. *Adv. Energy Mater.* **2017**, *7*, 1700600.

(18) Herz, L. M. How Lattice Dynamics Moderate the Electronic Properties of Metal-Halide Perovskites. *J. Phys. Chem. Lett.* **2018**, *9*, 6853−6863.

(19) Mozur, E. M.; Trowbridge, J. C.; Maughan, A. E.; Gorman, M. J.; Brown, C. M.; Prisk, T. R.; Neilson, J. R. Dynamical Phase Transitions and Cation Orientation-Dependent Photoconductivity in $CH(NH_2)_2PbBr_3$. *ACS Mater. Lett.* **2019**, *1*, 260−264.

(20) Ptak, M.; Sieradzki, A.; Simenas, M.; Maczka, M. Molecular Spectroscopy of Hybrid Organic-Inorganic Perovskites and Related Compounds. *Coord. Chem. Rev.* **2021**, *448*, 214180.

(21) Zhou, Y.; Zhou, Z.; Chen, M.; Zong, Y.; Huang, J.; Pang, S.; Padture, N. P. Doping and Alloying for Improved Perovskite Solar Cells. *J. Mater. Chem. A* **2016**, *4*, 17623−17635.

(22) Ono, L. K.; Juarez-Perez, E. J.; Qi, Y. Progress on Perovskite Materials and Solar Cells with Mixed Cations and Halide Anions. *ACS Appl. Mater. Interfaces* **2017**, *9*, 30197−30246.

(23) Simenas, M.; Balciunas, S.; Svirskas, S.; Kinka, M.; Ptak, M.; Kalendra, V.; Gagor, A.; Szewczyk, D.; Sieradzki, A.; Grigalaitis, R.; et al. Phase Diagram and Cation Dynamics of Mixed $MA_{1-x}FA_xPbBr_3$ Hybrid Perovskites. *Chem. Mater.* **2021**, *33*, 5926−5934.

(24) Yao, H.; Zhao, J.; Li, Z.; Ci, Z.; Jin, Z. Research and Progress of Black Metastable Phase $CsPbI_3$ Solar Cells. *Mater. Chem. Front.* **2021**, *5*, 1221−1235.

(25) Pei, Y.; Liu, Y.; Li, F.; Bai, S.; Jian, X.; Liu, M. Unveiling Property of Hydrolysis-Derived $DMAPbI_3$ for Perovskite Devices: Composition Engineering, Defect Mitigation, and Stability Optimization. *iScience* **2019**, *15*, 165−172.

(26) Anelli, C.; Chierotti, M. R.; Bordignon, S.; Quadrelli, P.; Marongiu, D.; Bongiovanni, G.; Malavasi, L. Investigation of Dimethylammonium Solubility in $MAPbBr_3$ Hybrid Perovskite:

Synthesis, Crystal Structure, and Optical Properties. *Inorg. Chem.* **2019**, *58*, 944−949.
(27) Simenas, M.; Balciunas, S.; Wilson, J. N.; Svirskas, S.; Kinka, M.; Garbaras, A.; Kalendra, V.; Gagor, A.; Szewczyk, D.; Sieradzki, A.; et al. Suppression of Phase Transitions and Glass Phase Signatures in Mixed Cation Halide Perovskites. *Nat. Commun.* **2020**, *11*, 5103.
(28) Hsu, H.-L.; Chang, C.-C.; Chen, C.-P.; Jiang, B.-H.; Jeng, R.-J.; Cheng, C.-H. High-Performance and High-Durability Perovskite Photovoltaic Devices Prepared using Ethylammonium Iodide as an Additive. *J. Mater. Chem. A* **2015**, *3*, 9271−9277.
(29) Peng, W.; Miao, X.; Adinolfi, V.; Alarousu, E.; El Tall, O.; Emwas, A.-H.; Zhao, C.; Walters, G.; Liu, J.; Ouellette, O.; et al. Engineering of $CH_3NH_3PbI_3$ Perovskite Crystals by Alloying Large Organic Cations for Enhanced Thermal Stability and Transport Properties. *Angew. Chem., Int. Ed.* **2016**, *55*, 10686−10690.
(30) Shi, Z.; Zhang, Y.; Cui, C.; Li, B.; Zhou, W.; Ning, Z.; Mi, Q. Symmetrization of the Crystal Lattice of $MAPbI_3$ Boosts the Performance and Stability of Metal-Perovskite Photodiodes. *Adv. Mater.* **2017**, *29*, 1701656.
(31) Wu, C.; Chen, K.; Guo, D. Y.; Wang, S. L.; Li, P. G. Cations Substitution Tuning Phase Stability in Hybrid Perovskite Single Crystals by Strain Relaxation. *RSC Adv.* **2018**, *8*, 2900−2905.
(32) Nishi, K.; Oku, T.; Kishimoto, T.; Ueoka, N.; Suzuki, A. Photovoltaic Characteristics of $CH_3NH_3PbI_3$ Perovskite Solar Cells Added with Ethylammonium Bromide and Formamidinium Iodide. *Coatings* **2020**, *10*, 410.
(33) Kim, M.; Figueroa-Tapia, J. M.; Prato, M.; Petrozza, A. Engineering Multiphase Metal Halide Perovskites Thin Films for Stable and Efficient Solar Cells. *Adv. Energy Mater.* **2020**, *10*, 1903221.
(34) Simenas, M.; Balciunas, S.; Gagor, A.; Pieniazek, A.; Tolborg, K.; Kinka, M.; Klimavicius, V.; Svirskas, S.; Kalendra, V.; Ptak, M.; et al. Mixology of $MA_{1-x}EA_xPbI_3$ Hybrid Perovskites: Phase Transitions, Cation Dynamics, and Photoluminescence. *Chem. Mater.* **2022**, *34*, 10104−10112.
(35) Maczka, M.; Ptak, M.; Gagor, A.; Stefanska, D.; Zareba, J. K.; Sieradzki, A. Methylhydrazinium Lead Bromide: Noncentrosymmetric Three-Dimensional Perovskite with Exceptionally Large Framework Distortion and Green Photoluminescence. *Chem. Mater.* **2020**, *32*, 1667−1673.
(36) Maczka, M.; Gagor, A.; Zareba, J. K.; Stefanska, D.; Drozd, M.; Balciunas, S.; Simenas, M.; Banys, J.; Sieradzki, A. Three-Dimensional Perovskite Methylhydrazinium Lead Chloride with Two Polar Phases and Unusual Second-Harmonic Generation Bistability above Room Temperature. *Chem. Mater.* **2020**, *32*, 4072−4082.
(37) Mączka, M.; Ptak, M.; Fedoruk, K.; Stefańska, D.; Gągor, A.; Zaręba, J. K.; Sieradzki, A. The Lattice Symmetrization Worked, but With a Plot Twist: Effects of Methylhydrazinium Doping of $MAPbI_3$ on Phase Transitions, Cation Dynamics and Photoluminescence. *J. Mater. Chem. C* **2024**, *12*, 1396−1405.
(38) Petrosova, H. R.; Kucheriv, O. I.; Shova, S.; Gural'skiy, I. A. Aziridinium Cation Templating 3D Lead Halide Hybrid Perovskites. *Chem. Commun.* **2022**, *58*, 5745−5748.
(39) Mączka, M.; Ptak, M.; Gągor, A.; Zaręba, J. K.; Liang, X.; Balčiūnas, S.; Semenikhin, O. A.; Kucheriv, O. I.; Gural'skiy, I. A.; Shova, S.; et al. Phase Transitions, Dielectric Response, and Nonlinear Optical Properties of Aziridinium Lead Halide Perovskites. *Chem. Mater.* **2023**, *35*, 9725−9738.
(40) Saliba, M.; Matsui, T.; Domanski, K.; Seo, J.-Y.; Ummadisingu, A.; Zakeeruddin, S. M.; Correa-Baena, J.-P.; Tress, W. R.; Abate, A.; Hagfeldt, A.; et al. Incorporation of Rubidium Cations Into Perovskite Solar Cells Improves Photovoltaic Performance. *Science* **2016**, *354*, 206−209.
(41) Kieslich, G.; Sun, S.; Cheetham, A. K. Solid-State Principles Applied to Organic-Inorganic Perovskites: New Tricks for an Old Dog. *Chem. Sci.* **2014**, *5*, 4712−4715.
(42) Simenas, M.; Gagor, A.; Banys, J.; Maczka, M. Phase Transitions and Dynamics in Mixed Three- and Low-Dimensional Lead Halide Perovskites. *Chem. Rev.* **2024**, *124*, 2281−2326.
(43) Ke, W.; Stoumpos, C. C.; Spanopoulos, I.; Mao, L.; Chen, M.; Wasielewski, M. R.; Kanatzidis, M. G. Efficient Lead-Free Solar Cells Based on Hollow {en}$MASnI_3$ Perovskites. *J. Am. Chem. Soc.* **2017**, *139*, 14800−14806.
(44) Ke, W.; Stoumpos, C. C.; Zhu, M.; Mao, L.; Spanopoulos, I.; Liu, J.; Kontsevoi, O. Y.; Chen, M.; Sarma, D.; Zhang, Y.; et al. Enhanced Photovoltaic Performance and Stability with a New Type of Hollow 3D Perovskite {en}$FASnI_3$. *Sci. Adv.* **2017**, *3*, No. e1701293.
(45) Ke, W.; Stoumpos, C. C.; Spanopoulos, I.; Chen, M.; Wasielewski, M. R.; Kanatzidis, M. G. Diammonium Cations in the $FASnI_3$ Perovskite Structure Lead to Lower Dark Currents and More Efficient Solar Cells. *ACS Energy Lett.* **2018**, *3*, 1470−1476.
(46) Ke, W.; Spanopoulos, I.; Tu, Q.; Hadar, I.; Li, X.; Shekhawat, G. S.; Dravid, V. P.; Kanatzidis, M. G. Ethylenediammonium-Based "Hollow" Pb/Sn Perovskites with Ideal Band Gap Yield Solar Cells with Higher Efficiency and Stability. *J. Am. Chem. Soc.* **2019**, *141*, 8627−8637.
(47) Spanopoulos, I.; Ke, W.; Stoumpos, C. C.; Schueller, E. C.; Kontsevoi, O. Y.; Seshadri, R.; Kanatzidis, M. G. Unraveling the Chemical Nature of the 3D "Hollow" Hybrid Halide Perovskites. *J. Am. Chem. Soc.* **2018**, *140*, 5728−5742.
(48) Lu, J.; Jiang, L.; Li, W.; Li, F.; Pai, N. K.; Scully, A. D.; Tsai, C.-M.; Bach, U.; Simonov, A. N.; Cheng, Y.-B.; Spiccia, L. Diammonium and Monoammonium Mixed-Organic-Cation Perovskites for High Performance Solar Cells with Improved Stability. *Adv. Energy Mater.* **2017**, *7*, 1700444.
(49) Leblanc, A.; Mercier, N.; Allain, M.; Dittmer, J.; Fernandez, V.; Pauporté, T. Lead- and Iodide-Deficient $(CH_3NH_3)PbI_3$ (d-MAPI): The Bridge between 2D and 3D Hybrid Perovskites. *Angew. Chem., Int. Ed.* **2017**, *56*, 16067−16072.
(50) Leblanc, A.; Mercier, N.; Allain, M.; Dittmer, J.; Pauporté, T.; Fernandez, V.; Boucher, F.; Kepenekian, M.; Katan, C. Enhanced Stability and Band Gap Tuning of α-$[HC(NH_2)_2]PbI_3$ Hybrid Perovskite by Large Cation Integration. *ACS Appl. Mater. Interfaces* **2019**, *11*, 20743−20751.
(51) Gollino, L.; Leblanc, A.; Dittmer, J.; Mercier, N.; Pauporté, T. New Dication-Based Lead-Deficient 3D $MAPbI_3$ and $FAPbI_3$ "d-HPs" Perovskites with Enhanced Stability. *ACS Omega* **2023**, *8*, 23870−23879.
(52) Tsai, C.-M.; Lin, Y.-P.; Pola, M. K.; Narra, S.; Jokar, E.; Yang, Y.-W.; Diau, E. W.-G. Control of Crystal Structures and Optical Properties with Hybrid Formamidinium and 2-Hydroxyethylammonium Cations for Mesoscopic Carbon-Electrode Tin-Based Perovskite Solar Cells. *ACS Energy Lett.* **2018**, *3*, 2077−2085.
(53) Spanopoulos, I.; Hadar, I.; Ke, W.; Guo, P.; Mozur, E. M.; Morgan, E.; Wang, S.; Zheng, D.; Padgaonkar, S.; Manjunatha Reddy, G. N.; et al. Tunable Broad Light Emission from 3D "Hollow" Bromide Perovskites through Defect Engineering. *J. Am. Chem. Soc.* **2021**, *143*, 7069−7080.
(54) Worku, M.; Tian, Y.; Zhou, C.; Lin, H.; Chaaban, M.; jin Xu, L.; He, Q.; Beery, D.; Zhou, Y.; Lin, X.; et al. Hollow Metal Halide Perovskite Nanocrystals with Efficient Blue Emissions. *Sci. Adv.* **2020**, *6*, No. eaaz5961.
(55) Grater, L.; Wang, M.; Teale, S.; Mahesh, S.; Maxwell, A.; Liu, Y.; Park, S. M.; Chen, B.; Laquai, F.; Kanatzidis, M. G.; et al. Sterically Suppressed Phase Segregation in 3D Hollow Mixed-Halide Wide Band Gap Perovskites. *J. Phys. Chem. Lett.* **2023**, *14*, 6157−6162.
(56) Jayanthi, K.; Spanopoulos, I.; Zibouche, N.; Voskanyan, A. A.; Vasileiadou, E. S.; Islam, M. S.; Navrotsky, A.; Kanatzidis, M. G. Entropy Stabilization Effects and Ion Migration in 3D "Hollow" Halide Perovskites. *J. Am. Chem. Soc.* **2022**, *144*, 8223−8230.
(57) Senocrate, A.; Spanopoulos, I.; Zibouche, N.; Maier, J.; Islam, M. S.; Kanatzidis, M. G. Tuning Ionic and Electronic Conductivities in the "Hollow" Perovskite {en}$MAPbI_3$. *Chem. Mater.* **2021**, *33*, 719−726.
(58) Hwang, J. S.; Lin, K. J.; Tien, C. Measurement of Heat Capacity by Fitting the Whole Temperature Response of a Heat-Pulse Calorimeter. *Rev. Sci. Instrum.* **1997**, *68*, 94−101.

https://doi.org/10.1021/acs.chemmater.4c01346
Chem. Mater. 2024, 36, 7397−7405

(59) Maczka, M.; Zienkiewicz, J. A.; Ptak, M. Comparative Studies of Phonon Properties of Three-Dimensional Hybrid Organic-Inorganic Perovskites Comprising Methylhydrazinium, Methylammonium, and Formamidinium Cations. *J. Phys. Chem. C* **2022**, *126*, 4048−4056.
(60) Maczka, M.; Ptak, M. Temperature-Dependent Raman Studies of $FAPbBr_3$ and $MAPbBr_3$ Perovskites: Effect of Phase Transitions on Molecular Dynamics and Lattice Distortion. *Solids* **2022**, *3*, 111−121.
(61) Shao, F.; Qin, P.; Wang, D.; Zhang, G.; Wu, B.; He, J.; Peng, W.; Sum, T. C.; Wang, D.; Huang, F. Enhanced Photovoltaic Performance and Thermal Stability of $CH_3NH_3PbI_3$ Perovskite through Lattice Symmetrization. *ACS Appl. Mater. Interfaces* **2019**, *11*, 740−746.
(62) He, J.; Li, T.; Liu, X.; Su, H.; Ku, Z.; Zhong, J.; Huang, F.; Peng, Y.; Cheng, Y.-B. Influence of Phase Transition on Stability of Perovskite Solar Cells Under Thermal Cycling Conditions. *Sol. Energy* **2019**, *188*, 312−317.
(63) Fabini, D. H.; Hogan, T.; Evans, H. A.; Stoumpos, C. C.; Kanatzidis, M. G.; Seshadri, R. Dielectric and Thermodynamic Signatures of Low-Temperature Glassy Dynamics in the Hybrid Perovskites $CH_3NH_3PbI_3$ and $HC(NH_2)_2PbI_3$. *J. Phys. Chem. Lett.* **2016**, *7*, 376−381.
(64) Govinda, S.; Kore, B. P.; Bokdam, M.; Mahale, P.; Kumar, A.; Pal, S.; Bhattacharyya, B.; Lahnsteiner, J.; Kresse, G.; Franchini, C.; et al. Behavior of Methylammonium Dipoles in $MAPbX_3$ (X = Br and I). *J. Phys. Chem. Lett.* **2017**, *8*, 4113−4121.
(65) Cordero, F.; Craciun, F.; Trequattrini, F.; Imperatori, P.; Paoletti, A. M.; Pennesi, G. Competition between Polar and Antiferrodistortive Modes and Correlated Dynamics of the Methylammonium Molecules in $MAPbI_3$ from Anelastic and Dielectric Measurements. *J. Phys. Chem. Lett.* **2018**, *9*, 4401−4406.
(66) Mohanty, A.; Swain, D.; Govinda, S.; Row, T. N. G.; Sarma, D. D. Phase Diagram and Dielectric Properties of $MA_{1-x}FA_xPbI_3$. *ACS Energy Lett.* **2019**, *4*, 2045−2051.
(67) Poglitsch, A.; Weber, D. Dynamic Disorder in Methylammoniumtrihalogenoplumbates (II) Observed by Millimeter-Wave Spectroscopy. *J. Chem. Phys.* **1987**, *87*, 6373−6378.
(68) Xu, Q.; Eguchi, T.; Nakayama, H.; Nakamura, N.; Kishita, M. Molecular Motions and Phase Transitions in Solid $CH_3NH_3PbX_3$ (X = C1, Br, I) as Studied by NMR and NQR. *Z. Naturforsch. A* **1991**, *46*, 240−246.
(69) Loidl, A.; Hemberger, J.; Winterlich, M.; Ries, H.; Böhmer, R. Linear and Nonlinear Dielectric Spectroscopy in Dipolar Glasses. *Ferroelectrics* **1996**, *176*, 43−59.
(70) Bokov, A. A.; Ye, Z.-G. Recent Progress in Relaxor Ferroelectrics with Perovskite Structure. *J. Mater. Sci.* **2006**, *41*, 31−52.
(71) Kleemann, W. Relaxor Ferroelectrics: Cluster Glass Ground State via Random Fields and Random Bonds. *Phys. Status Solidi (b)* **2014**, *251*, 1993−2002.
(72) van de Goor, T. W. J.; Liu, Y.; Feldmann, S.; Bourelle, S. A.; Neumann, T.; Winkler, T.; Kelly, N. D.; Liu, C.; Jones, M. A.; Emge, S. P.; et al. Impact of Orientational Glass Formation and Local Strain on Photo-Induced Halide Segregation in Hybrid Metal-Halide Perovskites. *J. Phys. Chem. C* **2021**, *125*, 15025−15034.
(73) Mozur, E. M.; Maughan, A. E.; Cheng, Y.; Huq, A.; Jalarvo, N.; Daemen, L. L.; Neilson, J. R. Orientational Glass Formation in Substituted Hybrid Perovskites. *Chem. Mater.* **2017**, *29*, 10168−10177.

https://doi.org/10.1021/acs.chemmater.4c01346
Chem. Mater. 2024, 36, 7397−7405